ACS APPLIED MATERIALS & INTERFACES

Research Article

www.acsami.org

Hexagonal Boron Nitride Coated Carbon Nanotubes: Interlayer Polarization Improved Field Emission

Han-Chen Chang, Hsin-Jung Tsai, Wen-Yi Lin, Yung-Chi Chu, and Wen-Kuang Hsu*

Department of Materials Science and Engineering, National Tsinghua University, HsinChu 30013, Taiwan

ABSTRACT: Coating of h-BN onto carbon nanotubes induces polarization at interfaces, and charges become localized at N and C atoms. Field emission of coated tubes is found to be highly stable, and current density fluctuates within 4%. Study further reveals that the electric field established between coatings and tubes facilitates charge transfer across interfaces and electrons are emitted through occupied and unoccupied bands of N and B atoms.

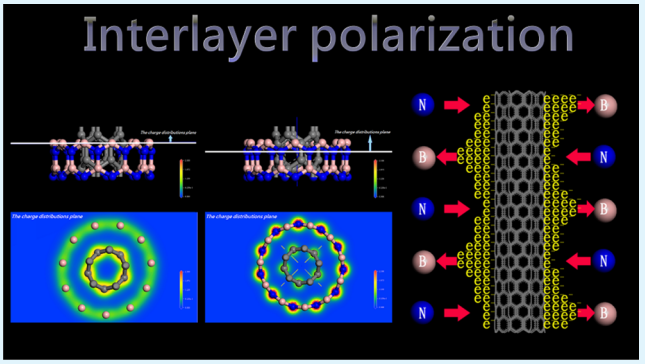

KEYWORDS: *carbon nanotubes, boron nitride, field emission, Fowler−Nordheim equation, ab initio calculation, Mulliken charge, interlayer polarization*

1. INTRODUCTION

Carbon nanotubes (CNTs) are a one-dimensional conductor made of rounded graphene sheets and do not suffer from the Peierls distortion at low temperature (T).[1,2] Upon bending, stresses can be rapidly dispersed through rigid networks and the s- and p-electrons rehybridize to prevent bond dissociation at strained lattices.[3−5] Theory has predicted that tube closure due to pentagons induced positive curvature may create additional states around Fermi level (E_F) and is expected to possess a greater density of states (DOS) than that elsewhere on tube. STM spectra confirm local DOS to be asymmetric, whereas a small gap is present between LUMO and HOMO levels, indicative of a semiconducting phase.[6] In the presence of an electric field, tube tips become negatively charged and filling of electrons into HOMO and LUMO states results in E_F upshift toward unoccupied band.[7] In other words, charged tubes have a reduced work function (ψ) and are expected to emit electrons at low turn-on field (E_{on}).[8]

Factors that determine the performance of field emission (FE) include current density (J) and emission stability; the former must reach a threshold field (E_{th} = 10 mA·cm^{-2}) for practical use and is controlled by ψ and field enhancement factor (β). The latter is often challenged by oxidation induced degradation and can be characterized by the degree of J fluctuation over a long period of time. For a single tube, J is low and β lies in 30−260. Large J however relies on multi-emission sources, such as CNT films and arrays of aligned tubes.[9] The study shows that emission from aggregated tubes barely degrades at low field (<1.3 V/μm) and obtained $I-V$ curves are consistent with the Fowler−Nordheim (F−N) model. J then rapidly saturates as the field exceeds 4.4 V/μm and β decreases, attributed to tip degradations.[10] Two factors account for J saturation; first, aggregation of CNTs induces screening effect and emission mainly comes from those that are long and are pointing to anode;[11] second, emission comes from defect states that are kinetically unstable at high field.[12] According to the Fermi−Dirac distribution, the energy spread in CNTs lies in 0.15−0.2 eV and contribution to J mainly comes from occupied states.[13] X-ray photoelectron spectra verify emission from π and $\sigma + \pi$ states, and both lie in 3−5 eV.[14] Study reveals that the B-doping created BC_3 state lies in the same energy regime and has been proved capable of emitting electrons at low E_{on}.[15] N-doping gives a similar result and the ψ due to E_F upshift toward unoccupied band is reduced.[16] Doping, however, causes breaking of hexagonal symmetry, and polarized lattices become vulnerable to O_2 attacks.

Hexagonal-phase BN (h-BN) is a wide bandgap semiconductor with a negative electron affinity.[17] The study indicates that BN nanotubes are isoelectronic and their FE characteristics include a single slope in F−N plot, stable J, and low oxidative damages.[17] Production of BN nanotubes however is difficult and current techniques rely on discharge, laser heating, pyrolysis, and C/BN substitution.[18−21] Other methods have also been developed to generate BN nanotubes in a large scale, such as catalytic chemical vapor deposition[22−24] and Ar assisted thermal reduction.[25] In fact, FE proceeds mainly through surface states and making of BN nanotubes is unnecessary. Su et al. have carried out emission tests on BN coated CNTs, and E_{on} is found to be 16.8 V·μm^{-1}.[26] This value decreases with reducing coating thickness, and measurements give

Received: April 22, 2015
Accepted: June 12, 2015
Published: June 12, 2015

DOI: 10.1021/acsami.5b03492
ACS Appl. Mater. Interfaces 2015, 7, 14456−14462

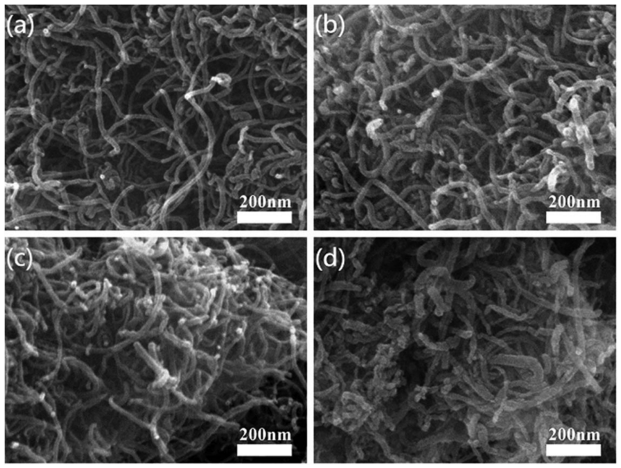

Figure 1. SEM images of CNTs (a) in comparison with C@BN_{100} (b), C@BN_{200} (c), and C@BN_{300} (d).

E_{on} = 4−6 V·μm^{-1} at 3−5 nm.[27] BN coatings however are cubic phase and can barely correlate with CNTs. Accordingly, emission induces significant heating at interface and J strongly fluctuates. In this work, CNTs are coated with h-BN and excellent FE is verified, including stable J and low E_{on}. The study further reveals that BN coating induces corrugated dispersion of charges at tube surfaces and emission proceeds through electron tunneling from CNTs to B 2p and N 2p states.

2. EXPERIMENTAL SECTION

BN coated multiwalled CNTs (MWCNTs) are prepared by chemical vapor deposition as follows. First, B_2O_3 powders (J. T. Baker) and MWCNTs (average diameter of ∼15 nm, length of ∼10 μm, C-Nano Technology Limited) are mixed in a pulverizing machine and the mixture is heated in a NH_3/Ar (1:4) flow at 1200 °C for 60 min. Second, samples are cooled in Ar flow and are subsequently dispersed in boiling water to remove residual oxides. Three sets of samples are made and are hereafter defined as C@BN_{100}, C@BN_{200}, and C@BN_{300} where numbers in lower case denote experiments carried out in 100, 200, and 300 sccm NH_3/Ar flows. Third, washed samples are dried at 70 °C and are characterized with various methods, including field emission scanning electron microscopy (FE-SEM) (JSE-6500F), thermogravimetric analysis (TGA) (PerkinElmer Pyris 1 TGA), X-ray diffraction (XRD) (Shimadzu XRD6000), chemical analysis (ESCA)

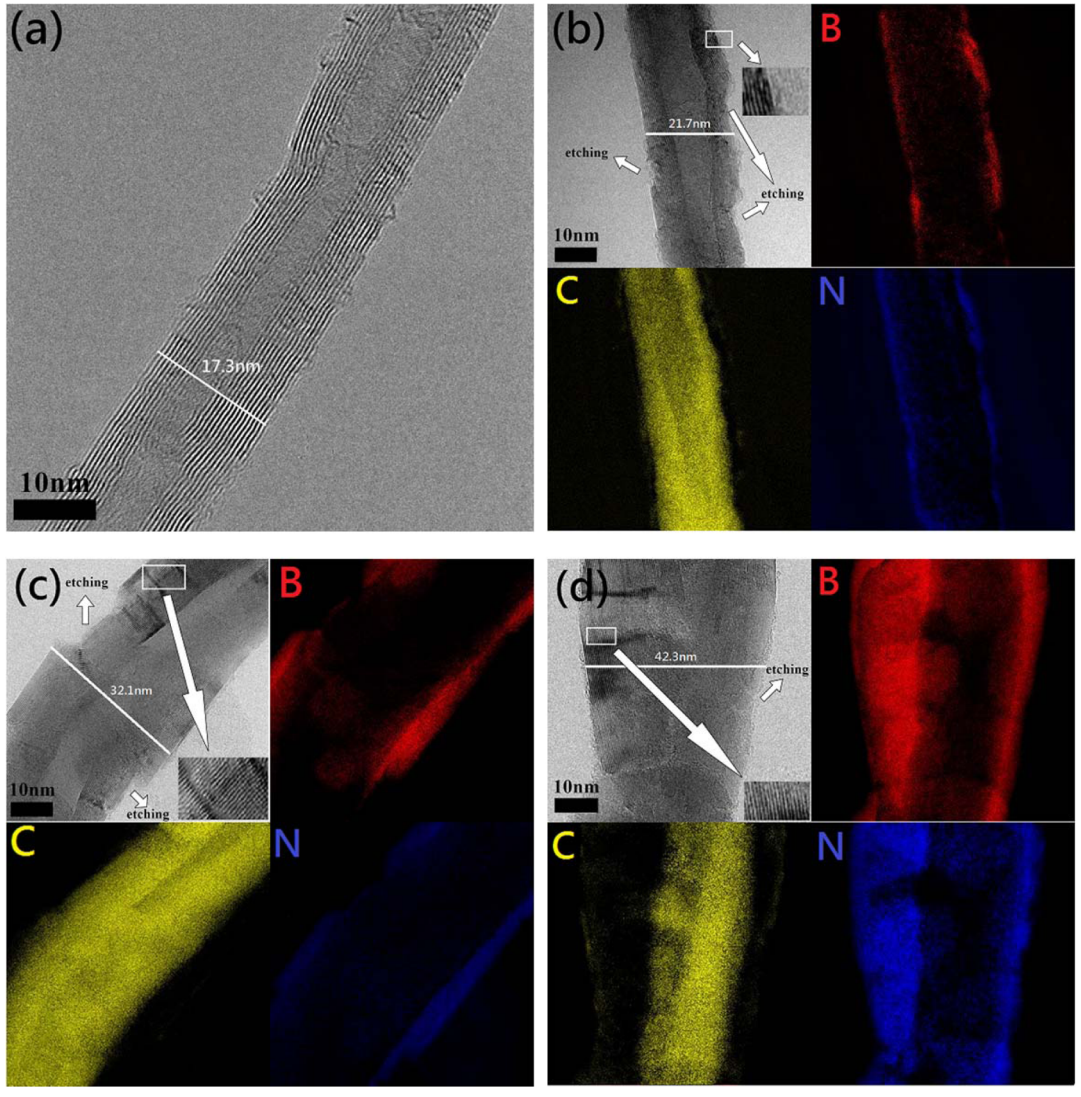

Figure 2. TEM images of pristine CNTs (a), C@BN_{100} (b), C@BN_{200} (c), and C@BN_{300} (d). The elemental boron, carbon, and nitrogen maps generated by EELS mapping of the TEM micrograph are also shown (top right, lower left and right, parts b−d). Insets and arrows indicate layered BN and etched edges.

DOI: 10.1021/acsami.5b03492
ACS Appl. Mater. Interfaces 2015, 7, 14456−14462

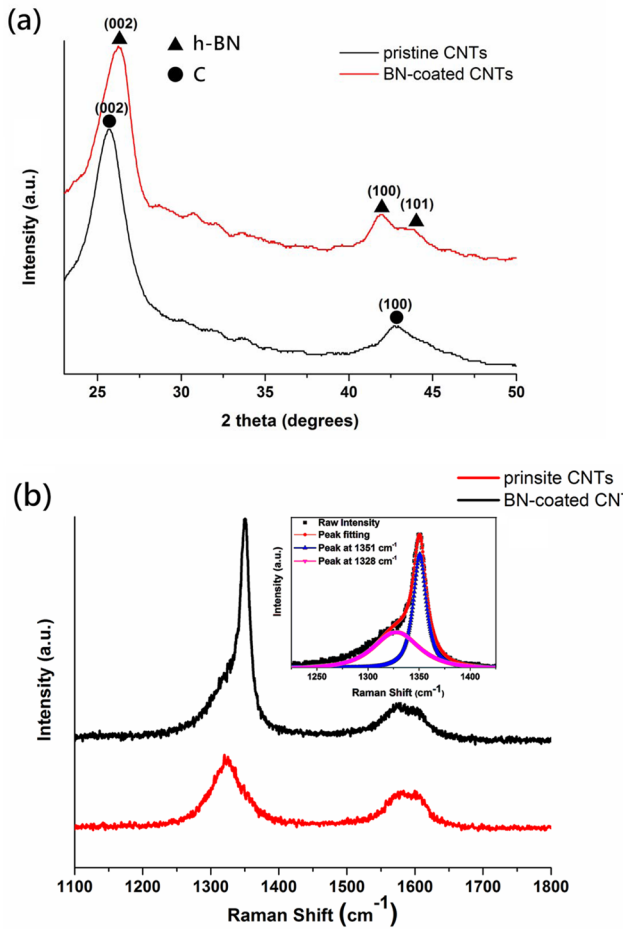

Figure 3. X-ray diffraction patterns (a) and Raman (b) of pristine CNTs and C@BN. Inset: fitted profiles of the main peak at 1320−1360 cm^{-1}.

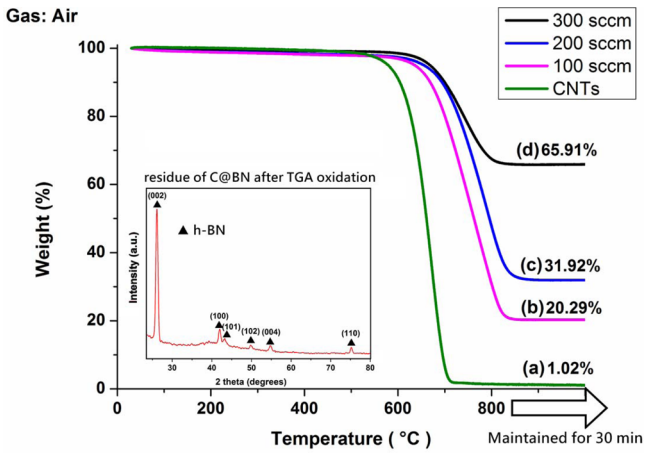

Figure 4. TGA profiles of CNT and C@BN tubes. Inset: XRD profile after TGA oxidation.

(Ulvac-PHI, PHI-1600), and high-resolution transmission electron microscopy (HRTEM) (FEI Tecnai, G2, F-20) equipped with an apparatus for parallel recording of electron energy loss spectroscopy (EELS). Thermogravimetric analyses (TGA, 10 °C/min) are carried out in air, and an empty crucible is used as reference. FE is measured in a high-vacuum chamber (10^{-7} Torr) using a spherical platinum tip as anode (1 mm in diameter), and J is recorded with a power supply (Keithley 2410, resolution of ±0.5 nA), the spacing between anode and samples being fixed at 100 μm. Ab initio calculation is performed to probe charge dispersion at BN/C interfaces, and procedures are briefed as follows. A double-walled zigzag CNT [(5,0)@(11,0)] is built within a 5 nm × 5 nm amorphous cell, and interlayer spacing is geometrically optimized to the van der Waal's regime. The outer tubule is then substituted with BN, and the Mulliken charge density is calculated using density function theory treated with exchange−correlation and Perdew ultrasoft pseudopotential. The tolerance threshold of self-consistent field is set at 10^{-6} eV per atom for structure convergence and 0.04 $Å^{-1}$ for the Monkhorst−Pack k-point grid separation.

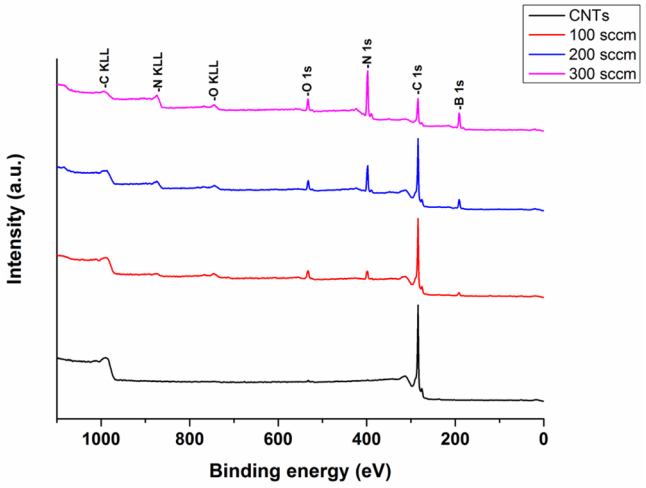

Figure 5. Full XPS spectra of the pristine CNTs and C@BN tubes synthesized at different flow rates.

Table 1. XPS Calculated Atomic Concentrations of B, C, and N

	atomic concentration (%)			
element	CNTs (%)	$C@BN_{100}$ (%)	$C@BN_{200}$ (%)	$C@BN_{300}$ (%)
B	0	8.66	17.17	35.85
C	99.92	83.84	66.60	31.73
N	0.08	7.5	16.23	32.42

3. RESULTS AND DISCUSSION

Figure 1 shows SEM images of CNTs (a), in comparison with $C@BN_{100}$ (b), $C@BN_{200}$ (c), and $C@BN_{300}$ (d). We find that reacted tubes exhibit rough surfaces, and roughness becomes obvious in $C@BN_{300}$ (Figure 1d). Pristine CNTs, in contrast, display clean surfaces, and amorphous carbons are barely seen (Figure 2a). TEM also verifies surfaces of $C@BN_{100}$ tubes to be scraggly (top left, Figure 2b), and EELS mapping indicates origin of roughness from BN coating (top right, lower left and right, Figure 2b). Core−shell structure is also present in $C@BN_{200}$ and $C@BN_{300}$, coating thickness being measured to be 4 ± 1 and 18 ± 3 nm (Figure 2c,d). BN has three types of structure, whereas only hexagonal phase with trigonal symmetry displays layered fringes in TEM, consistent with Figure 2b−d (insets). XRD and Raman support coatings to be layered BN: first, reflections at 2θ = 25.9°, 42.1°, and 43.6° come from crystallographic planes of (002), (100), and (101) (Figure 3a).[28] Second, CNTs made by pyrolysis are always defective and barely exhibit reflections arising from correlated hexagons between adjacent layers, i.e. (101) and (103).[29] Accordingly, (101) seen in reacted tubes must arise from BN coatings (Figure 3a). Third, Raman profile at 1320−1360 cm^{-1} can be

DOI: 10.1021/acsami.5b03492
ACS Appl. Mater. Interfaces 2015, 7, 14456−14462

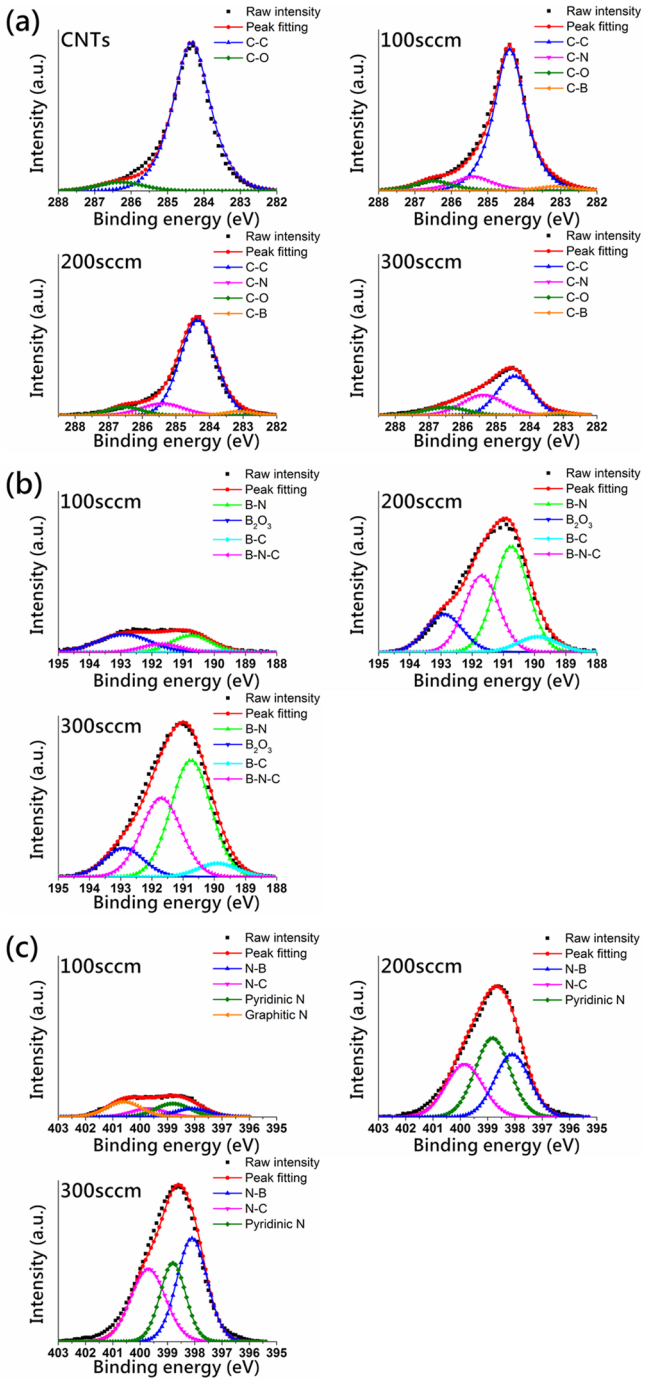

Figure 6. Deconvolution of the C 1s (a), B 1s (b), and N 1s (c) spectra of the C@BN synthesized at different flow rates.

deconvoluted into two peaks at 1328 and 1351 cm^{-1}; the former is the D-band from CNTs, and E_{2g} mode of h-BN is for the latter (Figure 3b).[22−24]

We find that BN coatings truly promote oxidative resistance, and improvement is supported by TGA (Figure 4) At T < 500 °C, CNT weight loss is small and comes from water evaporation and burning of carbonaceous impurities at tube surfaces. Tube oxidation begins at 550 °C and weight loss reaches 98% at 710 °C, along with trace of Fe_2O_3 arising from particle oxidation. BN coatings promote oxidation temperature to 640 °C, and large weight loss takes place at 700−800 °C. Again, coating thickness ∝ flow rate at a given reaction time is

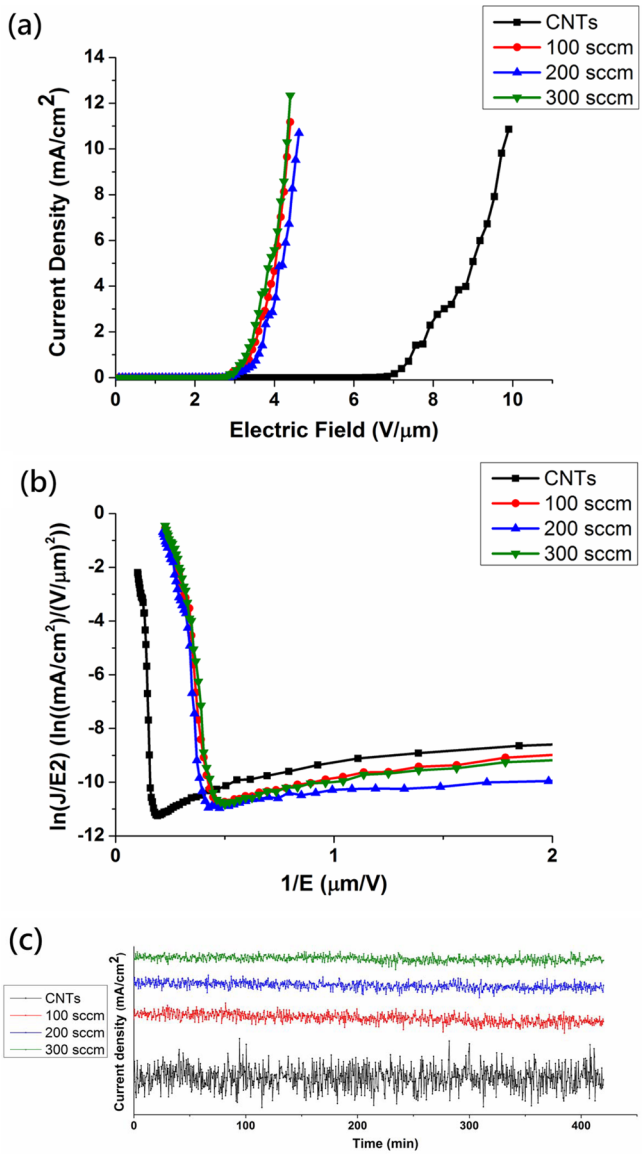

Figure 7. FE characteristics of CNT and C@BN tubes (a), F−N plot (b), and FE stability for a period of 7 h at 2 $mA{\cdot}cm^{-2}$ (c).

verified by increased yield of remaining h-BN at 820 °C, i.e., $C@BN_{100}$ (=20.29%) < $C@BN_{200}$ (=31.9%) < $C@BN_{300}$ (=65.9%). XPS spectra support TGA (Figure 5), atomic concentration based on integration of peaks at 190 eV (B 1s), 284 eV (C 1s), and 398 eV (N 1s) being measured to be C/BN of 7:1 for $C@BN_{100}$, 3:1 for $C@BN_{200}$, and 1:3 for $C@BN_{300}$ (Table 1).

BN formation according to analyses above may proceed through the following reactions.

$$B_2O_3 + 2C + 2NH_3 \rightarrow 2BNC + 3H_2O \quad (1)$$

$$2BNC + \frac{1}{2}B_2O_3 + NH_3 \rightarrow 3BN + 3CO_{(g)} + \frac{3}{2}H_2O \quad (2)$$

$$B_2O_3 + 2NH_3 \rightarrow 2BN + 3H_2O \quad (3)$$

Formation of intermediate (BNC) in the first and second reactions is consistent with etched tubes (C-mapping profiles, arrows, Figure 2b−d) and implies BN formation through CNTs acting as templates. Figure 6a displays C 1s spectra of CNTs

DOI: 10.1021/acsami.5b03492
ACS Appl. Mater. Interfaces 2015, 7, 14456−14462

Table 2. Comparison of FE Characteristics of C@BN Tubes with Related Structures and Data Obtained from CNTs

sample	V_{on} (V·μm^{-1})	E_{th} (V·μm^{-1})	β	ψ (eV)	J stability (fluctuation) (%)
uncoated CNTs	6.51 ± 0.02	9.82 ± 0.06	2370.51 ± 52	4.95	±25−30
h-BN-coated CNTs	2.66 ± 0.01	4.42 ± 0.01	3094.04 ± 63	2.8	±4−5
ZnO (particles) coated CNTs[39]	5 ± 0.01	8.18 ± 0.05	3651.87 ± 42	4.89	±3−4
MgO-coated CNTs[42]	4.96 ± 0.01	9.06 ± 0.05	2472.44 ± 51	3.25	±6−9
Ti-coated CNTs[41]	5.91 ± 0.02	7.33 ± 0.04	1097.27 ± 31	4.29	±10−15

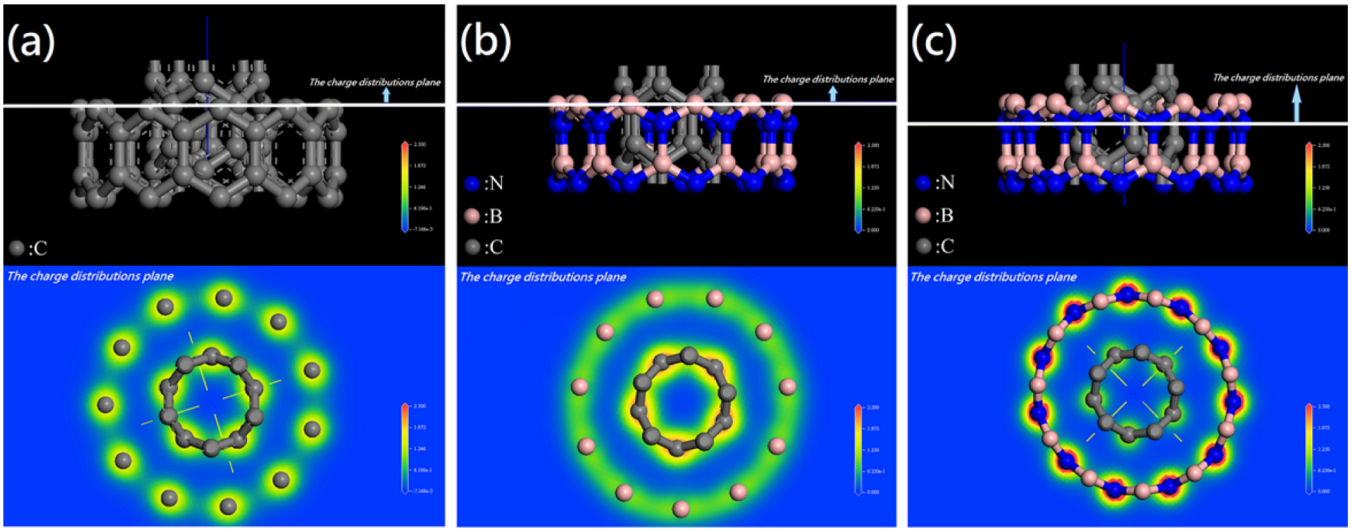

Figure 8. Mulliken charge distribution in bilayered CNT (a) and C@BN tubes with C−B (b) and C−N alignments (c).

and C@BN fabricated at different flow rates. For CNTs, profile consists of two peaks, including C−C bond at 284.3 eV and C−O bond at 286.2 eV (panel I, top left).[30,31] The C−B and C−N bonds emerge as tubes are coated, and energy lies at 283.1 and 285.7 eV, respectively (panels II−V (100−300 sccm, respectively), Figure 6a). The C−B and C−N profiles also appear at B 1s spectra, together with hexagonal B−N at 190.5 eV, B_2O_3 at 192.9 eV, and ternary B−N−C phase at 191.5 eV (Figure 6b).[32−34] Substitutions of C by B and N are further supported by emergence of pyridinic and graphitic N at 398.9 and 400.9 eV (N 1s spectra, Figure 6c).[30,31] Once the first BN layer forms, further reactions of B_2O_3 with NH_3 and CNTs are inhibited and subsequent production of BN proceeds through the third reaction. Again, coating thickness ∝ flow rate is evident by increased peak intensity of BN from $C@BN_{100}$ to $C@BN_{300}$ (Figure 6b,c).

Figure 7 shows FE characteristics of CNTs and C@BN tubes (a), and the F−N plots (b) are made according to equation below.[10]

$$\ln(J/E^2) = \ln(A\beta^2/\psi) + (-B\psi^{3/2}/\beta)(1/E)$$

where E is the electric field and, A and B are set as 1.56×10^{-10} A·eV·V^{-2} and 6.83×10^9 eV$^{-3/2}$·V·m^{-1}.[35] First, the linear F−N plot confirms electronic tunneling from emitters into vacuum in the presence of electric field (Figure 7b).[36,37] Second, measurements give E_{on} = 6.51 V·μm^{-1} for CNTs and 2.65−2.67 V·μm^{-1} for C@BN tubes, the E_{th} being measured to be 9.82 V·μm^{-1} and 4.41−4.43 V·μm^{-1} respectively. C@BN tubes with superior FE characteristics are also reflected in J profile over a period of 7 h at 2 mA·cm^{-2} (Figure 7c). Clearly, J is stable for C@BN tubes and fluctuates within ±4%. CNTs, in contrast, show strong fluctuations and J instability increases to ±25−30%, indicative of emission from various surface states (e.g., dangling edges, point defects, and oxygenated lattices).[38] Table 2 compares FE characteristics of C@BN tubes with related structures, along with data obtained from bare CNTs as reference. (i) Coating reduces E_{on} and E_{th} by 59% and 55% for C@BN, 23% and 17% for ZnO, 0.24% and 7% for MgO, and 9% and 25% for Ti coated tubes. (ii) The ψ decreases by 43% for C@BN, 1% for ZnO, 34% for MgO, and 13% for Ti coated tubes. Point i has been interpreted as a result of coating created emission channels which are slightly polarized.[39] FE through oxide coatings, however, implies charge transfer across interfaces. In this case, the E_F of CNTs must upshift in order to equalize with oxides, and ψ decreases accordingly [i.e., point ii]. E_F equalization is unlikely in the current study because BN is isoelectronic and is of 3.4 Å separation from CNTs. We find that BN coating induces polarization at interfaces and charges are highly localized at C and N atoms, respectively. Figure 8 shows the Mulliken charge distribution in bilayered CNT and C@BN tubes where lines denote electron density at termination edges. For CNT, charges evenly distribute over hexagonal networks, and density in both layers is identical (Figure 8a). Substitution of outer C layer by BN induces electron correlation, and charges redistribute along tube axis. First, C atoms are electron enriched as in line with B, charge density being 2-fold greater than that on bare CNTs (pink, Figure 8b). Second, C atoms become electron deficit in the next zigzag line and charges appear to localize at N atoms (blue, Figure 8c). Ionic nature of B−N bonds underlines corrugated dispersion of charges along CNT (Figure 9), and interlayer polarization accounts for ψ reduction. Note that calculation based on density functional theory reveals a similar result.[40]

High aspect ratio is often considered to be essential for emitter selection and has been proved to be true for nanotubes and nanowires.[10,39] BN coating, however, does not promote

DOI: 10.1021/acsami.5b03492
ACS Appl. Mater. Interfaces 2015, 7, 14456−14462

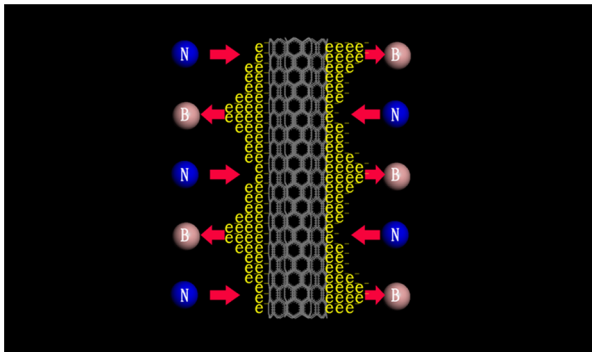

Figure 9. BN coating induced corrugated dispersion of charges along CNT.

CNT aspect ratio, and improved FE may therefore originate from enhanced local field at emitters. First, coating creates sharp edges and promotes β by 30% (Figure 2b,c and Table 2). Second, similar results also occur in ZnO (54%) and MgO coated tubes (4%) (Table 2). Note that coating, depending on cohesive energy of selected precursors and pretreatments of tubes, does not always produce fine particles on CNTs and deposition may occasionally result in continuous domains (i.e., thin films). In this case, local E is weakened and β decreases (i.e., Ti coated tubes, Table 2).[41] Finally, it is important to understand emission sites at C@BN and the study here suggests two possible channels, including N atoms in occupied and B atoms in unoccupied states. First, both are highly polarized in the presence of E, and second, they lie in the vicinity of E_F.[40]

4. CONCLUSION

CNTs are successfully coated with layered BN, and core−shell structure is verified by TEM, elemental mapping, XRD, and XPS. Coating induces polarization at interfaces, and charges are found to localize at C and N atoms. Interfacial polarization improves FE properties, including stability, E_{on}, E_{th}, and oxidative temperature. Electrons are most likely emitted through N atoms in occupied states and B atoms in unoccupied states, and J exceeds E_{th} at 4.5 V/μm.

AUTHOR INFORMATION

Corresponding Author

*Tel: +886-3-571-5131. Fax: +886-3-572-2366. E-mail: wkhsu@mx.nthu.edu.tw.

Notes

The authors declare no competing financial interest.

ACKNOWLEDGMENTS

We thank the Ministry of Science Technology of Taiwan for financial support under Grant MOST-103-2112-M-007-009-MY2.

REFERENCES

(1) Wong, E. W.; Sheehan, P. E.; Lieber, C. M. Nanobeam Mechanics: Elasticity, Strength, and Toughness of Nanorods and Nanotubes. *Science* **1997**, *277*, 1971−1975.

(2) Yu, M. F.; Lourie, O.; Dyer, M. J.; Moloni, K.; Kelly, T. F.; Ruoff, R. S. Strength and Breaking Mechanism of Multiwalled Carbon Nanotubes under Tensile Load. *Science* **2000**, *287*, 637−640.

(3) Yu, M. F.; Files, B. S.; Arepalli, S.; Ruoff, R. S. Tensile Loading of Ropes of Single Wall Carbon Nanotubes and Their Mechanical Properties. *Phys. Rev. Lett.* **2000**, *84*, 5552−5555.

(4) Bonard, J. M.; Weiss, N.; Kind, H.; Stöckli, T.; Forró, L.; Kern, K.; Châtelain, A. Tuning the Field Emission Properties of Patterned Carbon Nanotube Films. *Adv. Mater.* **2001**, *13*, 184−188.

(5) Wei, B. Q.; Vajtai, R.; Ajayan, P. M. Reliability and Current Carrying Capacity of Carbon Nanotubes. *Appl. Phys. Lett.* **2001**, *79*, 1172−1174.

(6) Carroll, D. L.; Redlich, P.; Ajayan, P. M.; Charlier, J. C.; Blase, X.; De Vita, A.; Car, R. Electronic Structure and Localized States at Carbon Nanotube Tips. *Phys. Rev. Lett.* **1997**, *78*, 2811−2814.

(7) Kim, C.; Kim, B.; Lee, S. M.; Jo, C.; Lee, Y. H. Electronic Structures of Capped Carbon Nanotubes under Electric Fields. *Phys. Rev. B* **2002**, *65*, 165418.

(8) Smith, R. C.; Forrest, R. D.; Carey, J. D.; Hsu, W. K.; Silva, S. R. P. Interpretation of Enhancement Factor in Nonplanar Field Emitters. *Appl. Phys. Lett.* **2005**, *87*, 013111.

(9) Bonard, J. M.; Dean, K. A.; Coll, B. F.; Klinke, C. Field Emission of Individual Carbon Nanotubes in the Scanning Electron Microscope. *Phys. Rev. Lett.* **2002**, *89*, 197602.

(10) Bonard, J. M.; Maier, F.; Stöckli, T.; Châtelain, A.; de Heer, W. A.; Salvetat, J. P.; Forró, L. Field Emission Properties of Multiwalled Carbon Nanotubes. *Ultramicroscopy* **1998**, *73*, 7−15.

(11) Bonard, J. M.; Salvetat, J. P.; Stöckli, T.; Forró, L.; Châtelain, A. Field Emission from Carbon Nanotubes: Perspectives for Applications and Clues to the Emission Mechanism. *Appl. Phys. A: Mater. Sci. Process.* **1999**, *69*, 245−254.

(12) Ding, J. J.; Lu, C. L.; Hsu, W. K. Capacitive Carbon Nanotube Networks in Polymer Composites. *Appl. Phys. Lett.* **2011**, *99*, 033111.

(13) de Heer, W. A.; Châtelain, A.; Ugarte, D. A Carbon Nanotube Field-Emission Electron. *Science* **1995**, *270*, 1179−1180.

(14) Bonard, J. M.; Croci, M.; Klinke, C.; Kurt, R.; Noury, O.; Weiss, N. Carbon Nanotube Films as Electron Field Emitters. *Carbon* **2002**, *40*, 1715−1728.

(15) Charlier, J. C.; Terrones, M.; Baxendale, M.; Meunier, V.; Zacharia, T.; Rupesinghe, N. L.; Hsu, W. K.; Grobert, N.; Terrones, H.; Amaratunga, G. A. J. Enhanced Electron Field Emission in B-Doped Carbon Nanotubes. *Nano Lett.* **2002**, *2*, 1191−1195.

(16) Zhong, Z.; Kang, J. K. Field Emission Performance of Nitrogen-Doped Carbon Nanotubes. *Electron. Mater. Lett.* **2007**, *3*, 7−11.

(17) Kimura, C.; Yamamoto, T.; Funakawa, S.; Hirakawa, M.; Murakami, H.; Sugino, T. Electron Field Emission from Boron Nitride Nanofilm and Its Application to Graphite Nanofiber. *J. Vac. Sci. Technol., B* **2003**, *21*, 2212−2216.

(18) Chopra, N. G.; Luyken, R. J.; Cherrey, K.; Crespi, V. H.; Cohen, M. L.; Louie, S. G.; Zettl, A. Boron Nitride Nanotubes. *Science* **1995**, *269*, 966−967.

(19) Goldberg, D.; Bando, Y.; Eremets, M.; Takemura, K.; Kurashima, K.; Tamiya, K.; Yusa, H. Boron Nitride Nanotube Growth Defects and Their Annealing-Out under Electron Irradiation. *Chem. Phys. Lett.* **1997**, *279*, 191−196.

(20) Han, W. Q.; Mickelson, W.; Cumings, J.; Zettl, A. Transformation of BxCyNz Nanotubes to Pure BN Nanotubes. *Appl. Phys. Lett.* **2002**, *81*, 1110−1112.

(21) Tang, C.; Bando, Y.; Sato, T. Catalytic Growth of Boron Nitride Nanotubes. *Chem. Phys. Lett.* **2002**, *362*, 185−189.

(22) Ahmad, P.; Khandaker, M. U.; Amin, Y. M. Effective Synthesis of Vertically Aligned Boron Nitride Nanotubes via a Simple CCVD. *Mater. Manuf. Processes.* **2014**, *30*, 706−710.

(23) Ahmad, P.; Khandaker, M. U.; Amin, Y. M. Synthesis of Vertically Aligned Flower-like Morphologies of BNNTs with the Help of Nucleation Sites in Co−Ni Alloy. *Mater. Sci. Semicond. Process.* **2015**, *38*, 113−118.

(24) Ahmad, P.; Khandaker, M. U.; Amin, Y. M. Synthesis of Highly Crystalline Multilayers Structures of ^{10}BNNTs as a Potential Neutron Sensing Element. *Ceram. Int.* **2015**, *41*, 4544−4548.

(25) Ahmad, P.; Khandaker, M. U.; Amin, Y. M. Synthesis of Boron Nitride Nanotubes by Argon Supported Thermal Chemical Vapor Deposition. *Phys. E (Amsterdam, Neth.)* **2015**, *67*, 33−37.

DOI: 10.1021/acsami.5b03492
ACS Appl. Mater. Interfaces 2015, 7, 14456−14462

(26) Su, C. Y.; Juang, Z. Y.; Chen, Y. L.; Leou, K. C.; Tsai, C. H. The Field Emission Characteristics of Carbon Nanotubes Coated by Boron Nitride Film. *Diamond Relat. Mater.* **2007**, *16*, 1393−1397.
(27) Yoo, J. B.; Han, J. H.; Choi, S. H.; Lee, T. Y.; Park, C. Y.; Jeong, T. W.; Lee, J. H.; Yu, S.; Park, G.; Yi, W. K.; Kim, H. S.; Baik, Y. J.; Kim, J. M. Emission Characteristics of Boron Nitride Coated Carbon Nanotubes. *Phys. B (Amsterdam, Neth.)* **2002**, *323*, 180−181.
(28) Han, W.; Bando, Y.; Kurashima, K.; Sato, T. Synthesis of Boron Nitride Nanotubes from Carbon Nanotubes by a Substitution Reaction. *Appl. Phys. Lett.* **1998**, *73*, 3085−3087.
(29) Oh, W. C.; Zhang, F. J.; Chen, M. L. Characterization and Photodegradation Characteristics of Organic Dye for Pt−Titania Combined Multi-Walled Carbon Nanotube Composite Catalysts. *J. Ind. Eng. Chem.* **2010**, *16*, 321−326.
(30) Chao, S.; Lu, Z.; Bai, Z.; Cui, Q.; Qiao, J.; Yang, Z.; Yang, L. Tuning Synthesis of Highly Active Nitrogen-doped Graphite and Determining the Optimal Structure from First-Principles Calculations. *Int. J. Electrochem. Sci.* **2013**, *8*, 8786−8799.
(31) Delpeux, S.; Beguin, F.; Benoit, R.; Erre, R.; Manolova, N.; Rashkov, I. Fullerene Core Star-like Polymers-1. Preparation from Fullerenes and Monoazidopolyethers. *Eur. Polym. J.* **1998**, *34*, 905−915.
(32) Essafti, A.; Gómez-Aleixandre, C.; Fierro, J. L. G.; Fernández, M.; Albella, J. M. Chemical Vapor Deposition Synthesis and Characterization of Co-Deposited Silicon−Nitrogen−Boron Materials. *J. Mater. Res.* **1996**, *11*, 2565−2574.
(33) Ramqvist, L.; Hamrin, K.; Johansson, G.; Fahlman, A.; Nordling, C. Charge Transfer in Transition Metal Carbides and Related Compounds Studied by ESCA. *J. Phys. Chem. Solids* **1969**, *30*, 1835−1847.
(34) Gómez-Aleixandre, C.; Essafti, A.; Albella, J. M. Kinetic Study of the Diborane/Methylamine Reaction: Composition and Structure of C−B−N Films. *J. Phys. Chem. B* **2000**, *104*, 4397−4402.
(35) Araki, H.; Katayama, T.; Yoshino, K. Field Emission from Aligned Carbon Nanotubes Prepared by Thermal Chemical Vapor Deposition of Fe-Phthalocyanine. *Appl. Phys. Lett.* **2001**, *79*, 2636−2638.
(36) Wang, G.; Wang, H.; Ling, Y.; Tang, Y.; Yang, X.; Fitzmorris, R. C.; Wang, C.; Zhang, J. Z.; Li, Y. Hydrogen-Treated TiO_2 Nanowire Arrays for Photoelectrochemical Water Splitting. *Nano Lett.* **2011**, *11*, 3026−3033.
(37) Lee, C. Y.; Lu, M. P.; Liao, K. F.; Lee, W. F.; Huang, C. T.; Chen, S. Y.; Chen, L. J. Free-Standing Single-Crystal $NiSi_2$ Nanowires with Excellent Electrical Transport and Field Emission Properties. *J. Phys. Chem. C* **2009**, *113*, 2286−2289.
(38) Li, Y. F.; Hung, C. I.; Li, C. C.; Chin, W.; Wei, B. Y.; Hsu, W. K. A Gas-Phase Hydrophilization of Carbon Nanotubes by Xenon Excimer Ultraviolet Irradiation. *J. Mater. Chem.* **2009**, *19*, 6761−6765.
(39) Green, J. M.; Dong, L.; Gutu, T.; Jiao, J.; Conley, J. F.; Ono, Y. ZnO-Nanoparticle-Coated Carbon Nanotubes Demonstrating Enhanced Electron Field-Emission Properties. *J. Appl. Phys.* **2006**, *99*, 094308.
(40) Chen, C. W.; Lee, M. H.; Lin, Y. T. Electro-Optical Modulation for a Boron Nitride Nanotube Probed by First-Principles Calculations. *Appl. Phys. Lett.* **2006**, *89*, 223105.
(41) Uh, H. S.; Park, S.; Kim, B. Enhanced Field Emission Properties From Titanium-Coated Carbon Nanotubes. *Diamond Relat. Mater.* **2010**, *19*, 586−589.
(42) Yi, W. K.; Jeong, T. W.; Yu, S. G.; Heo, J. N.; Lee, C. S.; Lee, J. H.; Kim, W. S.; Yoo, J. B.; Kim, J. M. Field-Emission Characteristics from Wide-Bandgap Material-Coated Carbon Nanotubes. *Adv. Mater.* **2002**, *14*, 1464−1468.

DOI: 10.1021/acsami.5b03492
ACS Appl. Mater. Interfaces 2015, 7, 14456−14462